Night-sky radiometry can revolutionize the characterization of light-pollution sources globally

Miroslav Kocifaj[a,b,1], Héctor Antonio Solano-Lamphar[c], and Gorden Videen[d]

[a]Institute of Construction and Architecture, Slovak Academy of Sciences, 845 03 Bratislava, Slovak Republic; [b]Faculty of Mathematics, Physics, and Informatics, Comenius University, 842 48 Bratislava, Slovak Republic; [c]Instituto de Investigaciones Dr. José María Luis Mora, Centro Interdisciplinario de Estudios Metropolitanos, Cátedras Consejo Nacional de Ciencia y Tecnología, 03730 Cuidad de México, México; and [d]Battlefield Environment Division, Army Research Laboratory, Adelphi, MD 20783

The city emission function (CEF), describing the angular emission from an entire city as a light source, is one of the key elements in night-sky radiance models. The CEF describes the rate at which skyglow depends on distance and is indispensable in any prediction of light-pollution propagation into nocturnal environments. Nevertheless, the CEF remains virtually unexplored because appropriate retrieval tools have been unavailable until very recently. A CEF has now been obtained from ground-based night-sky observations and establishes an experiment successfully conducted in the field to retrieve the angular emission function for an urban area. The field campaign was conducted near the city of Los Mochis, Mexico, which is well isolated from other cities and thus dominates all light emissions in its vicinity. The experiment has proven that radiometry of a night sky can provide information on the light output pattern of a distant city and allows for systematic, full-area, and cost-efficient CEF monitoring worldwide. A database of CEFs could initiate a completely new phase in light-pollution research, with significant economy and advanced accuracy of night-sky brightness predictions. The experiment and its interpretation represent unique progress in the field and contribute to our fundamental understanding of the mechanism by which direct and reflected uplight interact while forming the CEF.

skyglow | night-sky radiometry | light-pollution sources | upward emission function

Light pollution is spreading rapidly over the globe, primarily due to excessive use of artificial sources with elevated emissions in some parts of the visible spectrum. Some fraction of this light unintentionally or intentionally radiates directly into the upper atmosphere. Bright areas with outdoor lighting systematically increase from year to year as identified by both Earth-observing satellites and detector networks at ground level (1, 2). It is well documented that rays emitted by artificial lights can travel horizontally over long distances before reaching the ground and cause luminance of otherwise dark regions. Light pollution is a major problem in the field of astronomy— indeed, much of the pioneering work was performed with this in mind (3–8)—and it continues to attract attention in this field (e.g., ref. 9). Although the intensity of a light beam can significantly decay while it is transported through a turbid atmospheric environment (10), the role of air pollution remains one of the greatest unknown elements in skyglow theories (11).

Night-sky radiance from distant sources of light can vary over several orders of magnitude depending on the loading and nature of aerosol particles. The amplitude of these effects scale in magnitude with the radiant intensity function of a ground-based light source (12, 13); this function is the city emission function (CEF) (14), also known as the upward emission function. The CEF is a key property in modeling light pollution propagating through nocturnal environments (15). Until recently this function was only inferred indirectly or simulated conventionally using Garstang's equation (16), which was later modified by Cinzano et al. (17). Theoretically, the CEF also can be determined from satellite and airborne observations. The latter have been made, for example in Berlin, but they are limited to near-zenith emissions (18). Satellite measurements are useful to validate different CEF models, but as noted by Cinzano et al. (19), "at low elevation angles the spread is much too large to constrain adequately the function shape." The use of airborne platforms, including inexpensive drones, has the potential to impact the field substantially.

An empirical form of the CEF, obtained as a linear combination of reflected and direct emissions upward, has appeared useful in estimating the overall effect of artificial light sources at night (20), but it has to be emphasized that the CEF may vary significantly due to the individual nature of light emission and blocking urban constructs. Due to theoretical difficulties in modeling complex urban environments, some simplifications have been introduced in the forms of blocked and unblocked fractions of light, in which both are used to modify the original Garstang's equation (13). However, the analytical or empirical models only attempt to reduce the level of complexity and explain the basic features of light-emitting urban areas, rather than characterizing the wide diversity of angular emission patterns. Therefore, a method for in situ retrieval of the CEF is needed to enhance characterization of light emissions on a local scale and to verify models.

A method to determine the CEF using night-sky brightness measurements provides an opportunity to determine emission functions systematically over the world and also to reproduce a wide range of sky-radiance distributions (21). The method

Significance

Anthropogenic skyglow is currently a serious threat to natural environments near human settlements; however, a spread of light over wide areas is difficult to predict due to uncertainties in the city emission function (CEF) from many light sources. The CEF determines the rate at which skyglow varies with distance to a light source but remains virtually unexplored because appropriate retrieval tools have been unavailable. However, we have now obtained the CEF from ground-based night-sky radiometry and conducted a successful experiment to retrieve the CEF of an urban area. The method provides information on the CEF and allows for its systematic full-area economic monitoring while initiating a phase in light-pollution research.

presented here could lead to new CEF retrievals over many cities and towns in different territories. The technique is numerically fast, experimentally simple, and cost-efficient and uses routinely measured data; thus, it has great potential as a CEF solver for world-wide night-sky light pollution. While light pollution is the primary motivation of such studies, baseline clear-sky CEFs also provide the possibility of monitoring aerosol loading above cities and identification of sources of air pollution. The method to retrieve the CEF of cities is described comprehensively in *SI Appendix*. It should be clear that the results obtained for a single city cannot be generalized to other cities, and normally more than one measurement is needed to constrain the CEF to an acceptable level of measurement error.

Results

The night-sky radiance measured in the city of Los Mochis is shown in Fig. 1*C* as dots (for blue filter), crosses (for green filter), and triangles (for red filter), while the theoretical fits are displayed as dashed lines. The latter were obtained based on the CEF functions determined through numerical inversion; first the experimental data were used to retrieve the CEFs for each of the three spectral bands and then the theoretical radiance pattern was computed using emission functions as inputs to the model. A comparison of both the experimental and numerically simulated radiance data provides insight into the performance and success

of the method used. The above analysis is necessary because the retrieval procedure can produce instability under some circumstances, or the solution function may be unrealistic (e.g., having spikes or negative values). This is why the results have to be compared with the dataset to validate the method.

The cumulative radiant intensity functions in red and blue tend to decrease steeply as emission zenith angle approaches 80° (Fig. 2*A*; compare with dashed lines for Lambertian radiators), but for green the emission function has a completely different form showing an evident peak at about $z_E \approx 60°$ (Fig. 2 *A* and *B*). Although the CEF is shown here in arbitrary units, the coefficients of proportionality are the same for all colors.

The different emission functions found for different red, green, and blue colors emerge as a challenge for the light-pollution community. The emission in red is approximately double that of blue and green. However, a peak emission in green requires more attention. The red filter's spectral sensitivity function peaks at about 600 to 620 nm, which is well within the dominant emissions of HPS (high-pressure sodium) luminaires widely used in industrial and public lighting. In fact, different types of lamps and luminaires are part of the public lighting system of Los Mochis. Currently, the government is carrying out an action plan in the municipality with the aim of meeting the needs of night lighting and promoting energy saving in public lighting installations through a massive change of technology
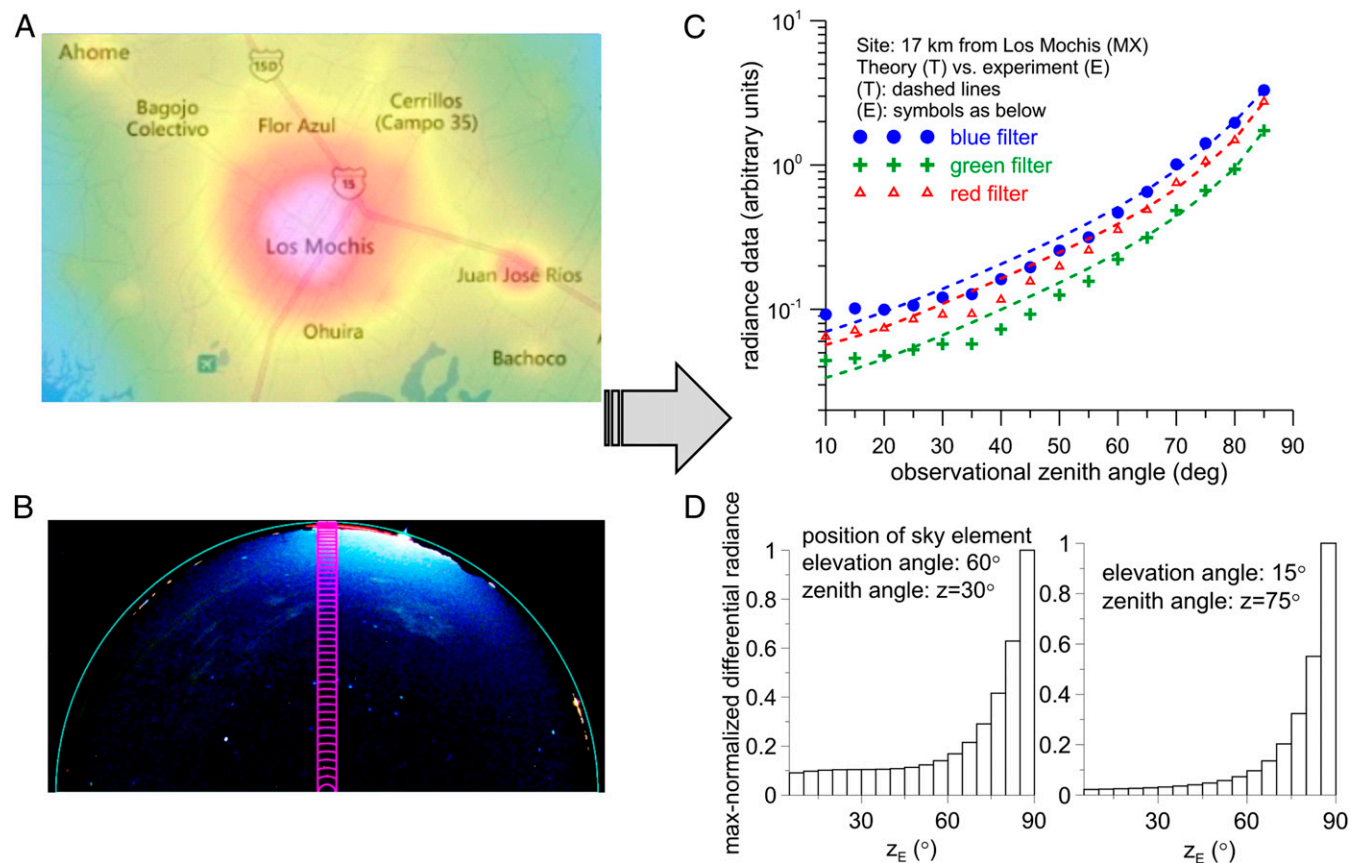
Fig. 1. The ground-based experiment on CEF retrieval was performed near the city of Los Mochis, Mexico. The topography of the most important light sources surrounding the measurement site (*A*) was retrieved from the sky brightness map produced with data from ref. 44 (https://www.lightpollutionmap.info). Radiance data were collected from zenith toward the light source at the horizon 17 km from the city. (*B*) An example of how the experimental data have been collected. The green line represents the location of the horizon. The magenta squares representing the FOV of the camera making the radiometric measurements are not aligned with a meridian passing through the brightest part of the light dome attributable to Los Mochis. (*C*) The measured values in blue, green, and red parts of the visible spectrum are compared against theoretical predictions that are shown here as dashed lines. (*D*) The contributions to the theoretical radiance from all ground-based light emissions are shown for two sky elements 60° and 15° above the horizontal. The emission angle is measured from the surface normal, so 0° means the photons are directed toward the zenith.
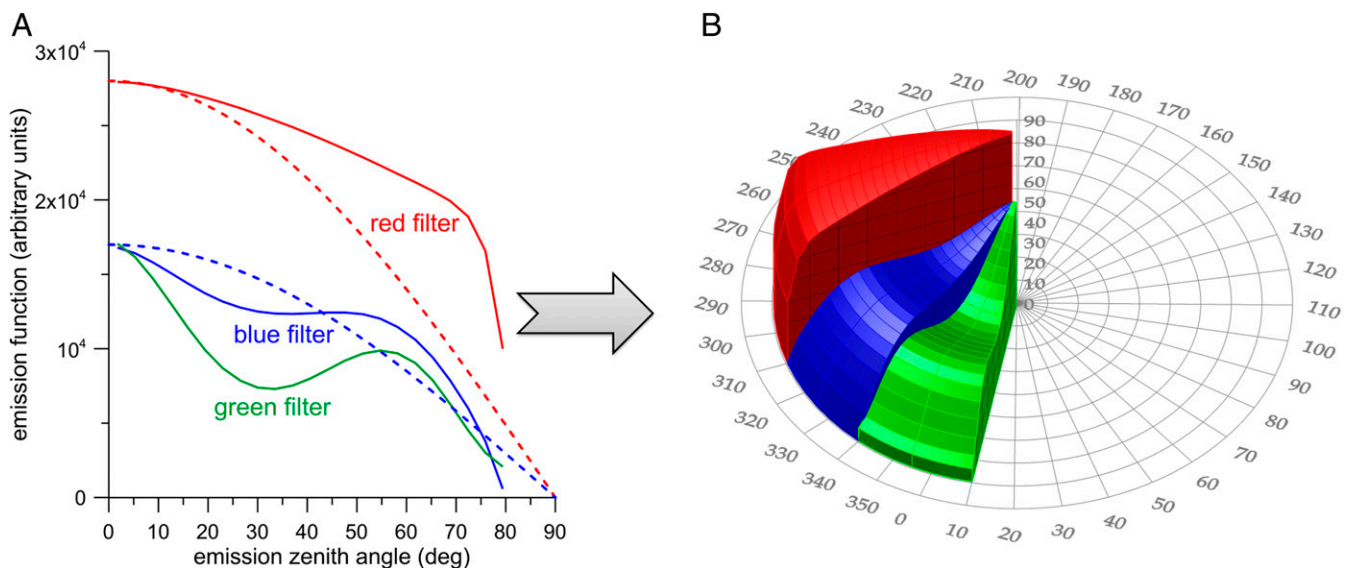
Fig. 2. Angular emission pattern of the city of Los Mochis in three colors inferred from night-sky radiance data. (*A*) The CEF as a function of emission zenith angle for blue, green, and red filters, respectively (solid lines). For comparison, the emission functions for Lambertian radiators are shown as dashed lines. (*B*) CEFs in spherical coordinates (3D plots) to get a better visualization of the spatial distribution of the radiant intensity distribution.

utilizing white LEDs. However, HPS vapor lamps are the main component of the original lighting system. Assuming HPS is a dominant source of light in the city, the signal measured using the green filter is expected to be half of that detected with the red filter. Note that the spectral response of the green filter drops to half of its maximum when transitioning from 530 nm to 600 nm (22). The abundant presence of red in the spectral power distribution (SPD) of urban lights is one of the most probable causes of the red-to-green ratio found here. The lack of blue in the SPD is typical of many light sources (23); thus, a low blue-to-red ratio is not surprising. The blue wavelength content is low in traditional street lighting, but Fig. 2 indicates the blue and green emissions are well balanced in the city. We suspect this is because of the employment of a new generation of LED lamps that are now the modern alternative to incumbent systems; other sources like metal halides are obsolete and almost unused in Los Mochis. Currently, the street-lighting transition to LEDs has attracted the general attention of city planners and designers because of potential energy savings; however, LED conversion can also have a number of negative consequences on both local and global scales (24). For instance, LED technology is known to have disruptive effects on astronomical observations, biodiversity, and even humans (25, 26). Blue light more than other wavelengths is intensively scattered backward and sideways in the Earth's atmosphere, thus making the night sky brighter and bluish (27). Blue light emissions from LEDs may disrupt melatonin production and impose an unacceptable burden on living creatures (28, 29).

A thorough investigation of the public lighting system has confirmed that the LED conversion of the city of Los Mochis is in progress, which is consistent with what has emerged from the inversion of radiance data (see the results for blue filter in Fig. 2). The CEF for red light decreases monotonically with increasing z_E, but slower than predicted from Lambert's cosine law (Fig. 2*A*). No doubt the CEF in red also includes reflection from ground surfaces and direct emission upward from luminaires and building interiors. The latter is especially important because interiors are often illuminated using unshielded lamps, which also produce thermal radiation. A secondary emission peak identified in the green color at about $z_E = 60°$ is an unexpected feature. However, the city of Los Mochis has abundant vegetation, with

natural enhanced reflection in the green. Many of the deciduous trees or plants reflect effectively in green (30) and in combination with directional leaf reflectance can produce a lobed reflectance pattern (31) with intensified emission to intermediate zenith angles. This directional reflectance from the green infrastructure appears the most likely mechanism for why the peak values of the CEF occur at angle $z_E = 60°$. Trees can be treated as ordinary light-reflecting urban elements for green light which can amplify flux emitted upward, depending on factors like chlorophyll (Chl) concentration (32) or nutrient availability (33). This green light is a vegetation-reflection signature, which can provide information on the content of trees, bushes, and other green flora within the urban landscape. When transitioning from green to red, the reflectance of broadleaves can either decrease in the case where the Chl *a* concentration is high or result in considerable increase in the case where the Chl *a* concentration is as low as tens of milligrams per square meter (34). The lowered Chl *a* levels are therefore another reason for the relatively abundant red light, as was discussed earlier in respect to the possible effect of lighting technology.

To examine the convergence of the inversion method we have analyzed data recorded at additional distances. Unfortunately, only one additional measurement satisfied most of the quality criteria, and it was acquired at a distance ∼1*D* from the city of Los Mochis, which is below the limit of 2*D* postulated later in this paper (*Data Acquisition*). This could impact the information content of the experimental data because of the physical constraints of the model. The radiance data for blue were excluded from further processing because of the dominance of Rayleigh scattering. Nevertheless, the method still provides good results (see dashed lines for two filters in Fig. 3) that asymptotically approach those shown in Fig. 2 (solid lines). A proper functionality of the underlying physics even beyond the applicable range of input values is a good indicator of the method's potential. The results presented are an example demonstrating the method's capability. It should be understood that multiple measurements have to be conducted to retrieve a well-constrained CEF for any specific city.
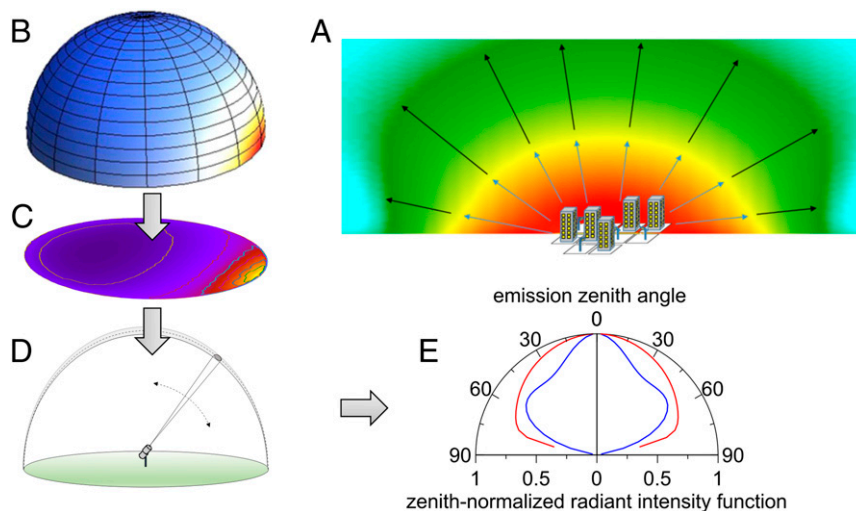
Methods

Artificial light escaping from cities is partially due to direct upward emission and partially due to reflection from underlying arbitrarily oriented surfaces
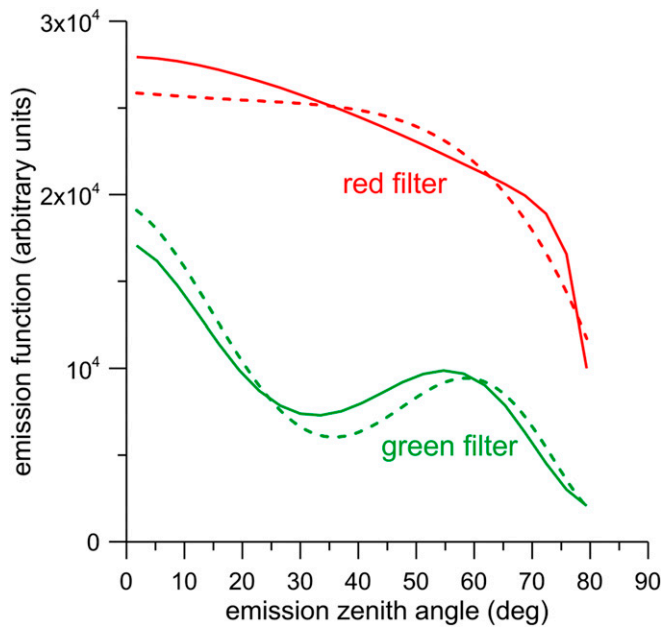
Fig. 3. Light output patterns as determined from inversion of sky radiance datasets taken at two distinct distances from the city: 17 km (solid lines) and 7 km (dashed lines). The radiance in blue has been excluded due to Rayleigh scatter dominance of back-scattered light recorded at short distances from the city.

(35). Light-emitting elements such as luminous building façades, outdoor area lighting, street lighting, electronic signs, billboards, and also the lights from cars are all characterized by different light output patterns that interfere in a nontrivial way, while contributing to the total radiant intensity distribution of an urban area. In addition, these other kinds of light-emitting or -reflecting surfaces do not behave like point sources and therefore are especially difficult to model in terms of constructing realistic CEFs. Because of varying urban and atmospheric conditions, the angular distribution of light is not constant near the artificially lit area, especially if the emission

function is examined at distances that are comparable to, or slightly exceed, any characteristic dimension of that area (see the yellow contour in Fig. 4A). However, as the distance increases, the function smoothly approaches that of the CEF (e.g., the outer boundaries of green area shown in Fig. 4A). There are really two regimes around cities: one very close to (and within) the city in which the angular structure of the CEF is strongly sensitive to individual sources and one at a much larger distance from the city in which the contributions of individual sources become indistinguishable from one another (compare two-color diagrams in Fig. 4A).

Principles. The idea behind sky-radiance analysis in terms of the CEF is fundamental to electromagnetic scattering theories that determine the radiance field everywhere if the properties of both the source of light and scattering medium are known. This core principle has proven to be the driving force for an ambitious project to develop a method that can be used to determine the CEF systematically for many cities over the world. The theoretical solution that introduces a linear, compact operator mapping between radiance data and CEF has been developed only recently (21) and requires the clear-sky radiance data to be taken at a local meridian that intersects a horizontal circle at the azimuthal position of a radiating city or town (Fig. 4 B–D). Fig. 4 B and C are representations of all-sky views, one shown as a hemisphere and the other as a circle in a plane. The angular distance between discrete sky elements, that is, the increment in zenith angle, cannot be arbitrarily small; otherwise, the algebraic equations would become linearly dependent. This can occur in solving inverse problems in which the kernels of the integral equation can overlap if the data grid is too dense (36).

Data Acquisition. The regularization technique used to retrieve the CEF is primarily designed for a dominant, well-isolated city or town but is also applicable for more complex systems in which a few approximately equally important emitters are closely spaced. However, the iterative scheme for retrieval of two or more CEFs concurrently is nontrivial. For this reason, it is preferable that the data be acquired in a locality where the upwardly directed light emissions from one dominant source exceed those produced by other nearby light sources. The inversion algorithm has been validated for sensitivity and specificity in the reproduction of the initial emission functions (21). The effects of experimental errors on retrieval accuracy are discussed in *SI Appendix*.

An experiment was performed near the city of Los Mochis, Mexico (Fig. 1A). The field campaign includes a set of measurements at distances not exceeding 10D, where D is the characteristic dimension of the light-emitting urban area. The inversion procedure also requires that the distance should not fall below ∼2D to keep the information content of the data high (21).

Fig. 4. Night-sky radiometry as a source of information on the angular emission pattern from whole-city light sources. (A–E) From theory to experimental and numerical determinations of the CEF. The light escaping from a city propagates in all directions, but with different intensity ratios (A) that depend on many factors, including urban design, spatial arrangement and technology of artificial lights, reflectivity of ambient surfaces, and atmospheric conditions including pollution levels (see also main text). Some fraction of photons emitted upward is scattered into the atmospheric environment and redirected downward while forming a bright dome of light over a city (B). The sky radiance distribution (C) taken under clear-sky conditions can be analyzed as a function of angular distance to the source of light (D) and interpreted in terms of the CEF (E) by applying an inverse operator on the data recorded. Two examples of the CEF are displayed in E.

Kocifaj et al.

ASTRONOMY

ENVIRONMENTAL SCIENCES

That property can be understood better when dealing with density functions that show the contribution of all ground emissions to the radiance in a specific element of the sky (Fig. 1D). Density functions (also referred to here as differential radiances) are plotted as histograms with data normalized to their maximum value. The bars represent the relative contributions of the CEF to the theoretical sky radiance 60° above the azimuthal position of a radiating city (Fig. 1D, Left). The corresponding bar diagram for sky radiance 15° above the horizontal is shown in Fig. 1D, Right.

Both diagrams demonstrate that sky radiance near a bright dome of light is influenced by emissions at low and/or intermediate angles z_E more than other radiance data. Of course, the form of the density function depends on input parameters, such as CEF shape, aerosol characteristics, and distance to the city. The sample computations made here are for an asymmetry parameter of 0.2, meaning that the mean radius of aerosol particles is as small as 0.1 µm. These can be compared with the aerosol optical properties computed in ref. 37. The optical depth of 0.1 along with the small size of aerosol particles is representative for most rural, natural, or even mountain regions. The single scattering albedo is as large as 0.9.

All sky images taken on-site provide brightness in red, green, and blue at central (nominal) wavelengths of 600 nm, 530 nm, and 460 nm, respectively. Data manipulation was necessary to limit the field of view (FOV) to ~2° to avoid blurring the information contained in the sky radiance patterns; otherwise, the angular distribution of the scattered light would be inaccurate. However, the FOV cannot be arbitrarily small (e.g., the size of a single photon-counting pixel at the photosensitive detector) because the potential imperfections in signals detected could make the inversion of radiance data inaccurate or even impossible. Thus, averaging over a set of nearby pixels is a reasonable approach to eliminate most systematic and random errors. This can be done numerically by evaluating the radiance gradient when transitioning from inner to outer pixels, or by resampling to a coarser scale.

Data Processing. Clear-sky conditions are a basic prerequisite for making CEF inversion possible. Nevertheless, a perfect, cloud-free sky is very rare; thus, it is convenient to repeat the measurements on different bright nights, ideally at different distances from the city. The errors originating from high, invisible clouds or any unexpected intensity fluctuations are minimized in this way. The field experiment in Los Mochis includes sky scanning at nine different sites located 7 to 19 km from the city center, of which only two satisfy most of the above criteria. The distance of the measuring site was well within the bounds discussed in *Data Acquisition*. The FOV and grid density of the radiance data allow for linear inversion algorithms (38) that allow us to obtain the solution function subject to constraint within the error margin of the experimental data. However, a few thin cirrus clouds were located at the sky opposite to the azimuthal position of the dominant source of light. These data were filtered before inversion took place. Systematic analyses of kernel functions and differential radiances show that key information about the CEF is contained in the data taken in the brightest part of the sky from the zenith toward the light source at horizon (Fig. 1B). Therefore, the uncertainty in the remaining part of the radiance pattern has only low impact on the solution function. However, such deficiency should not be ignored in interpreting the resulting CEF.

The data preprocessing algorithm has been described by Kocifaj and Solano-Lamphar (39) and includes data conversion, lens calibration with respect to projection and sensitivity functions, determination of zero-level signal (a dark frame picture), and calibration of red, green, and blue signals at the sensor using the spectral sensitivity functions for a single sensor. The calibration constants for red, green, and blue channels were used to compare three-color CEFs.

Conclusions

The use of radiance data in determining the multicolor emission function is a great challenge for the light-pollution community, as the CEF obtained in this way can significantly improve predictions of the effects that outdoor artificial lighting has on sky brightness at different distances from a city. All predictions that exist in this field are limited in accuracy due to the uncertainty of the CEF. The emission function has often been estimated based on experiences or approximated by simple formulae, but real CEFs for regional cities and towns remained largely unexamined. We have demonstrated that the information content of night-sky radiance data is sufficient to retrieve the angular emission function from whole-city light sources if the aerosol properties (most typically aerosol optical depth and asymmetry factor) are known. This has great potential to revolutionize retrieval of the CEFs of cities globally. The development and systematic updating of the geographical picture of the CEF can fill the gap in light-pollution modeling and help to make accurate predictions of artificial light distribution under various meteorological conditions, aerosol loading, or cloud coverage. In comparison with direct aerial sensing of nighttime emissions from artificially lit surfaces (18), the method of night-sky radiometry used here is rapid and cost-efficient and does not necessarily require expensive apparati (e.g., ref. 40). The data also can be recorded by a well-calibrated camera (such as in refs. 41 and 42) or All-Sky Transmission Monitor (43). Hence a wide community of experts in the field, even well-equipped technicians and amateur observers, could contribute to building a world map of CEFs through the collection of radiance data on a local scale. Street lighting modernization is not an annual process; therefore, the light emission pattern slowly changes for a given city or town, thus implying that nighttime radiance measurements should preferably be repeated to update CEF status.

1. Kyba CCM, et al. (2015) Worldwide variations in artificial skyglow. *Sci Rep* 5:8409.
2. Bará S (2016) Anthropogenic disruption of the night sky darkness in urban and rural areas. *R Soc Open Sci* 3:160541.
3. Treanor PJSJ (1973) A simple propagation law for artificial night-sky illumination. *Observatory* 93:117–120.
4. Walker MF (1973) Light pollution in California and Arizona. *Publ Astron Soc Pac* 85:508–519.
5. Berry RL (1976) Light pollution in southern Ontario. *J R Astron Soc Can* 70:97–115.
6. Walker MF (1970) The California site survey. *Publ Astron Soc Pac* 82:672–698.
7. Treanor PJSJ, Salpeter ESJ (1972) A portable night-sky photometer. *Observatory* 92:96–99.
8. Bertiau FCSJ, de Graeve ESJ, Treanor PJSJ (1973) The artificial night-sky illumination in Italy. *Vatican Obs Publ* 1:159–179.
9. Duriscoe DM (2013) Measuring anthropogenic sky glow using a natural sky brightness model. *Publ Astron Soc Pac* 125:1370–1382.
10. Aubé M (2015) Physical behaviour of anthropogenic light propagation into the nocturnal environment. *Philos Trans R Soc Lond B Biol Sci* 370:20140117.
11. Kocifaj M, Kómar L (2016) A role of aerosol particles in forming urban skyglow and skyglow from distant cities. *Mon Not R Astron Soc* 458:438–448.
12. Luginbuhl CB, Lockwood GW, Davis DR, Pick K, Selders J (2009) From the ground up I: Light pollution sources in Flagstaff, Arizona. *Publ Astron Soc Pac* 121:185–203.
13. Luginbuhl C, et al. (2009) From the ground up II: Sky glow and near-ground artificial light propagation in Flagstaff, Arizona. *Publ Astron Soc Pac* 121:204–212.
14. Kocifaj M (2018) Towards a comprehensive city emission function (CCEF). *J Quant Spectrosc Radiat Transf* 205:253–266.
15. Solano-Lamphar HA (2018) The emission function of ground-based light sources: State of the art and research challenges. *J Quant Spectrosc Radiat Transf* 211:35–43.
16. Garstang RH (1986) Model for artificial night-sky illumination. *Publ Astron Soc Pac* 98:364–375.
17. Cinzano P, Falchi F, Elvidge CD, Baugh K (2000) The artificial night sky brightness mapped from DMSP satellite operational linescan system measurements. *Mon Not R Astron Soc* 318:641–657.
18. Kuechly HU, et al. (2012) Aerial survey and spatial analysis of sources of light pollution in Berlin, Germany. *Remote Sens Environ* 126:39–50.
19. Cinzano P, Falchi F, Elvidge CD, Baugh KE (2001) The artificial sky brightness in Europe derived from DMSP satellite data. *Proceedings of the International Astronomical Union* (International Astronomical Union, Paris), Vol 196, pp 95–102.
20. Falchi F, et al. (2016) The new world atlas of artificial night sky brightness. *Sci Adv* 2:e1600377.
21. Kocifaj M (2017) Retrieval of angular emission function from whole-city light sources using night-sky brightness measurements. *Optica* 4:255–262.
22. Jiang J, Liu D, Gu J, Susstrunk S (2013) What is the space of spectral sensitivity functions for digital color cameras? *2013 IEEE Workshop on Applications of Computer Vision (WACV)* (IEEE, Piscataway, NJ), pp 168–179.

23. Davies TW, Smyth T (2018) Why artificial light at night should be a focus for global change research in the 21st century. *Glob Change Biol* 24:872–882.

24. Kyba CCM, et al. (2017) Artificially lit surface of Earth at night increasing in radiance and extent. *Sci Adv* 3:e1701528.

25. Gaston KJ, Davies TW, Bennie J, Hopkins J (2012) Reducing the ecological consequences of night-time light pollution: Options and developments. *J Appl Ecol* 49: 1256–1266.

26. Gaston KJ, Bennie J, Davies TW, Hopkins J (2013) The ecological impacts of nighttime light pollution: A mechanistic appraisal. *Biol Rev Camb Philos Soc* 88:912–927.

27. Luginbuhl CB, Boley PA, Davies DR (2014) The impact of light source spectral power distribution on sky glow. *J Quant Spectrosc Radiat Transf* 139:21–26.

28. Falchi F, Cinzano P, Elvidge CD, Keith DM, Haim A (2011) Limiting the impact of light pollution on human health, environment and stellar visibility. *J Environ Manage* 92: 2714–2722.

29. Aubé M, Roby J, Kocifaj M (2013) Evaluating potential spectral impacts of various artificial lights on melatonin suppression, photosynthesis, and star visibility. *PLoS One* 8:e67798.

30. Gates DM, Keegan HJ, Schleter JC, Weidner VR (1965) Spectral properties of plants. *Appl Opt* 4:11–20.

31. Woolley JT (1971) Reflectance and transmittance of light by leaves. *Plant Physiol* 47: 656–662.

32. Carter GA, Knapp AK (2001) Leaf optical properties in higher plants: Linking spectral characteristics to stress and chlorophyll concentration. *Am J Bot* 88:677–684.

33. Baltzer JL, Thomas SC (2005) Leaf optical responses to light and soil nutrient availability in temperate deciduous trees. *Am J Bot* 92:214–223.

34. Blackburn GA (1999) Relationships between spectral reflectance and pigment concentrations in stacks of deciduous broadleaves. *Remote Sens Environ* 70:224–237.

35. Kolláth Z, Dömény A, Kolláth K, Nagy B (2016) Qualifying lighting remodelling in a Hungarian city based on light pollution effects. *J Quant Spectrosc Radiat Transf* 181: 46–51.

36. Horvath H, et al. (2002) Size distributions of particles obtained by inversion of spectral extinction and scattering measurements. *Optics of Cosmic Dust*, NATO Science Series, eds Videen G, Kocifaj M (Springer, New York), Vol 79, p 143.

37. Mishchenko MI, Travis LD (1994) Light scattering by polydispersions of randomly oriented spheroids with sizes comparable to wavelengths of observation. *Appl Opt* 33:7206–7225.

38. Twomey S (2002) *Introduction to the Mathematics of Inversion in Remote Sensing and Indirect Measurements* (Dover Publications, Mineola, NY).

39. Kocifaj M, Solano-Lamphar HA (2015) Retrieval of Garstang's emission function from all-sky camera images. *Mon Not R Astron Soc* 453:819–827.

40. Kocifaj M, Kómar L, Kundracik F (2018) PePSS–A portable sky scanner for measuring extremely low night-sky brightness. *J Quant Spectrosc Radiat Transf* 210:74–81.

41. Duriscoe DM, Luginbuhl CB, Moore CA (2007) Measuring night-sky brightness with a wide-field CCD camera. *Publ Astron Soc Pac* 119:192–213.

42. Jechow A, et al. (2018) Tracking the dynamics of skyglow with differential photometry using a digital camera with fisheye lens. *J Quant Spectrosc Radiat Transf* 209: 212–223.

43. Hänel A, et al. (2018) Measuring night sky brightness: Methods and challenges. *J Quant Spectrosc Radiat Transf* 205:278–290.

44. Falchi F, et al. (2016) Supplement to the New World Atlas of Artificial Night Sky Brightness. GFZ Data Services, 10.5880/GFZ.1.4.2016.001.

ASTRONOMY

ENVIRONMENTAL SCIENCES